Research Article | Vol. 32, No. 10 / 6 May 2024 / Optics Express 17593
Optics EXPRESS

Compact tunable 80 MHz repetition rate vacuum ultraviolet light source up to 10 eV: intracavity high harmonic generation by nonlinear reflection on a AlN nanofilm in a mode locked Ti:sapphire oscillator

E. SERES,[1,*] J. SERES,[1] L. MARTINEZ-DE-OLCOZ,[2] AND T. SCHUMM[1]

[1]Atominstitut - E141, Technische Universität Wien, Stadionallee 2, 1020 Vienna, Austria
[2]Instituto de Microelectrónica de Barcelona, IMB-CNM (CSIC), Campus UAB, Cerdanyola, 08193, Barcelona, Spain
[*]enikoe-judit-seres@tuwien.ac.at

Abstract: We report the realization of an intra-oscillator high harmonic source based on a Kerr lens mode locked Ti:sapphire laser running at 80 MHz repetition rate. A nonlinear medium consisting of an AlN nanofilm on a thin sapphire substrate is placed inside the oscillator cavity. The harmonics are generated, in reflection geometry, on the AlN nanofilm, directing the harmonic beam out of the cavity. Exploiting the benefits of this approach, a compact size, tunable, high repetition rate and coherent vacuum ultraviolet light source with a spectrum up to the 7th harmonic has been achieved. In particular, the powerful 5th harmonic covering the 145-163 nm range aims to be an attractive tunable light source for spectroscopical applications.

1. Introduction

Extending the operational wavelength range of femtosecond frequency combs (operating at around 100 MHz repetition rates) into the vacuum ultraviolet (VUV) enables high-precision spectroscopy of new important atomic and molecular transitions for testing quantum electrodynamics, photoemission spectroscopy [1,2] or looking for new atomic or nuclear clock transitions [3]. There is a special interest to develop VUV frequency combs in the 150 nm range for high precision spectroscopy of the ^{229m}Th isomer nuclear transition [4–10] and the atomic transitions of Th ions in a similar wavelength range [11]. This spectral range can be reached by the 5th harmonic of Ti:sapphire or the 7th harmonic of Yb-doped lasers. Realizing repetition rates of 10-100 MHz or even higher is advantageous to alleviate the space-charge effect in photoemission spectroscopy [2]. For high precision measurements in the VUV [12,13], higher repetition rates yield less comb lines and more power in each of them. Furthermore, a larger number of subsequent pulses makes the comb lines narrower, improves the signal/noise ratio and reduces data acquisition time. Nonlinear up-conversion into the VUV range at such high repetition rate can in principle be realized by frequency doubling using KBBF crystals. An advantage of this concept is the possibility of maintaining phase matching and high conversion efficiency, even in CW operation. Another way can be dispersive wave generation [14], however, in both cases, acceptable conversion efficiencies below the limit of 150 nm were only obtained by low repetition rate (kHz) laser systems [14–16]. Other perturbative VUV generation can be achieved by cascaded second and third harmonic generation [17] or four-wave mixing [18,19] using gases, but such methods are demonstrated at CW or low repetition rates. To reach shorter wavelengths while maintaining a high repetition rate, high harmonic (HH) generation is the most widely used method, driven by oscillators or multi-stage laser systems running at the required high repetition

#522309 https://doi.org/10.1364/OE.522309
Journal © 2024 Received 23 Feb 2024; revised 10 Apr 2024; accepted 11 Apr 2024; published 29 Apr 2024

Optics EXPRESS

rates. Compact Ti:sapphire oscillators can deliver suitable short pulses and sufficient peak power for the generation of lower order harmonics extracavity, on solid samples [20–22]. Larger laser systems, delivering larger intensity, can generate higher order harmonics extracavity in gases [1,23,24], however usually at lower, few MHz repetition rate. Unfortunately, these extra-cavity systems have very low conversion efficiency (in single-pass geometries) and do not make efficient use of the available pump power.

The conversion efficiency can be improved when the Ti:sapphire oscillator [3,25–29] or the multi-stage Yb:fiber laser system [8,30–32] is extended with an enhancement cavity and the HH source is placed into it. Enhancement cavities recycle the unused laser pulse for the next round. The highest intracavity laser power of multi-kW and the highest nW HH power per comb line was achieved with such laser systems [8]. However, it makes the concept bulky, complex and sensitive: Any losses inside the secondary cavity act against the enhancement and the secondary cavity needs to be matched to the primary oscillator in repetition rate, dispersion (and carrier envelope phase).

Building the HH source directly into the primary cavity of an oscillator carries the advantage of the high intracavity power but without the difficulty of the synchronization of the enhancement cavity. This concept was successfully realized based on Ti:sapphire [33] and Yb:YAG [34–36] oscillators using gas media as HH sources. These systems were running at low 9-17 MHz repetition rates to reach the necessary laser intensities for HH generation in gases.

Nevertheless, an additional difficulty is arisen during the intracavity generation of HH (enhancement cavity or intra-oscillator): the generated harmonics co-propagated with the laser beam and it was necessary to couple the HH beam out of the cavity while maintaining low loss for the laser beam. For this purpose, different output coupling techniques were tested; they all struggle with low output coupling efficiency or high losses in the cavity or fast degradation or difficult alignment. Very good reviews of the output coupling methods and descriptions of specific solutions can be found in [3,8,12,13,37–43].

Here we aim to realize a VUV laser source in a very compact way, by integrating the HH source into the primary (and only) cavity of a mode-locked, femtosecond, Ti:sapphire oscillator. Earlier realizations [33–36] as mentioned above were running at much lower repetition rate and used gas media for HH generation. However, when increasing repetition rates, the remaining ionized gas plasma can produce instabilities in the cavity [12] . To avoid this problem, we have used a solid HH medium instead of gas, which proved its usability in an enhancement cavity [29].

In this paper, we report the realization of an intra-oscillator HH source at high repetition rate of 80 MHz. It is based on a Ti:sapphire oscillator, and a second focus was inserted into its cavity for the HH source. The solid medium, serving as the HH source, is an AlN film coated on a thin sapphire substrate, which is placed in the second focus in Brewster angle. The harmonics are generated by nonlinear reflection on the thin film. Due to the applied reflection geometry, the generated harmonics propagate at different direction than the laser beam, eliminating the need for a separate output coupler. The underlying harmonic generation mechanism on the boundary of two materials (including the special case of vacuum-material boundary) was described in [44] and experimentally observed in [20,45–50].

We first describe the oscillator setup and briefly summarize the theoretical background of nonlinear reflection. After that, we report the characterization of the tunable laser oscillator and the tunable HH source. We propose an explanation for the appearance of a weak coherent super-continuum based on the experimental observations of the interference between the harmonic lines and the super-continuum. After demonstrating the successful implementation of the concept, finally, we discuss the achieved harmonic power and its recent limitations and the possibilities of scaling the intracavity and the generated harmonic power up.

Optics EXPRESS

2. Setup of the intra-oscillator HH source

The developed setup (Fig. 1(a)) was based on an earlier oscillator [52] and a second focus was inserted, similarly to [33] resulting on a compact arrangement on a 30 cm × 60 cm footprint (without the spectrometer). All around, we developed an oscillator cavity tunable between 750 and 800 nm with intracavity power up to 10 W, which was possible by using all broadband chirp mirrors, high reflectors and output couple. The Ti:sapphire crystal was pumped with a Laser Quantum finesse pure 16, frequency doubled Nd:YAG laser, which can provide a power up to 16 W at 532 nm. Its beam was focused (f = 60 mm) into a 4 mm long Ti:sapphire crystal, cooled down to 10 °C, by a thermoelectric cooler. Curved high reflector mirrors with 100 mm radius directed the oscillator beams to the shorter (0.77 m) and longer (1.1 m) arms under angles of 6° and 8°, respectively.

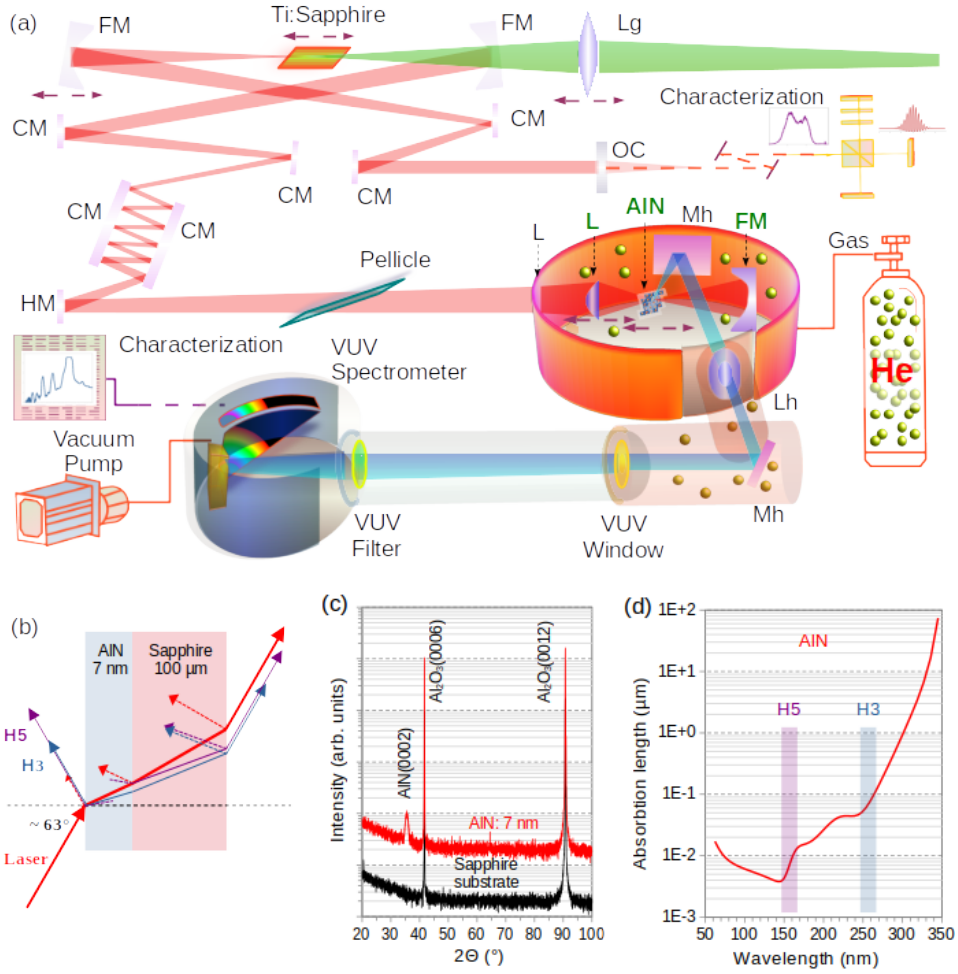

Fig. 1. (a) Setup of the Ti:sapphire oscillator with the intracavity HH source and spectrograph. CM: chirp mirror; HM: high reflector mirror; FM: focusing mirror; L, Lg, Lh: lenses for laser, green and harmonic beams; Mh: VUV mirror for the harmonic beam; (b) Reflections and refractions of the laser and harmonic beams on the AlN film on sapphire. (c) XRD characterization of AlN film and the substrate. (d) Calculated absorption lengths of AlN using the data from [51].

Optics EXPRESS

As first step, we designed an oscillator cavity by the guidelines of [53] and the second focus was inserted later. Two 1" chirped mirrors with 2 bounces/mirror and additional 1/2" chirped mirrors were needed to compensate the dispersions of the Ti:sapphire crystal and the air. All chirped mirrors had dispersion of -40 fs^2 (Layertec). A thin pellicle can be placed into the beam for tuning purpose (see next chapter). An output coupler with 1% transmission served to deliver small part of the intracavity beam for diagnostics like autocorrelation and spectrum measurements (results are presented below). This beam can also be used for repetition rate and carrier envelope phase stabilization.

As second step, we formed a second focus using a BK7 lens (f = 10 mm) and a high reflector mirror (R = 100 mm) at the end of the long arm. To compensate the dispersion of the intracavity focusing lens, the number of reflections on the 1" chirped mirror pair had to be increased from 2 to 5. To realize the HH source, a thin AlN film on a sapphire substrate was placed into the second focus in Brewster angle with the AlN film on the front surface. Films with different thicknesses were grown on 0.1 mm thick, EPI polished, c-cut (0001), VUV grade sapphire substrates. After cleaning the sapphire surface (Ar etching), AlN layers were deposited using the reactive RF magnetron sputtering technique, applying a power of 650W to a 8" diameter metallic Al target with 99.99% of purity. The working pressure was maintained at $5{\cdot}10^{-3}$ mbar with N_2 as the sole gas involved in the sputtering process. In this way, slow deposition rates were achieved (0.935 nm/min), enabling the deposition of such thin layers with the desired crystalline order. The crystal orientation of the AlN films were characterized by x-ray diffraction (XRD). As shown in the diffractogram of the 7 nm AlN film (Fig. 1(c)), only AlN (0002) Bragg peak (and those from Al_2O_3 substrate) are detected by XRD, indicating AlN (000l) orientation, without hints of other AlN peaks.

Since the refractive index of AlN ($n_{AlN} = 2.15$) [51] is not much larger than that of sapphire ($n_{sapphire} = 1.76$) [54] at near 800 nm, the corresponding Brewster angles 65° and 60° are similar enough for reaching a low <1% measured reflection loss at around 63°. Harmonics are generated on the front surface (surface layer) of the AlN film due to nonlinear refraction and nonlinear reflection. The most important occurring beam paths are presented in Fig. 1(b). At around the Brewster angle, only very small fractions of the incident laser beam are reflected from all the three possible interfaces. These beams are represented with dashed red arrows. The laser beam mainly passed through the AlN/sapphire substrate, experiencing only small losses. In the case of the multiple harmonics, the generation mechanism on the boundary of two materials was described in [44] and experimentally observed in reflection [45] and in transmission [20,46] from surfaces and from interfaces. Taking the boundary condition, the wave vectors should fulfill the condition [44,47]

$$k_{qx} = qk_{1x} \tag{1}$$

where k_q and k_1 are the wave numbers of the q-th harmonic and the fundamental ($q = 1$) laser beams and the x-axis is oriented along the boundary in the direction of the plane of incidence. Consequently, the reflected and transmitted harmonic beams obey

$$n_1(\omega_q)sin(\theta_{rq}) = n_2(\omega_q)sin(\theta_{tq}) = n_1(\omega_1)sin(\theta_i). \tag{2}$$

Here, θ_{rq} and θ_{tq} are the angles of the generated harmonic beams in the reflection and transmission directions and θ_i is the incident angle of the laser beam. According to Eq. (2), harmonics reflected from the front surface of the AlN film propagate in the same direction, as presented in Fig. 1(b), because in vacuum $n_1(\omega_q) = n_1(\omega_1) = 1$. However, inside the media, because of different refractive indexes, different harmonics propagate in different directions but leave the plan-parallel sample in the same direction with a slight lateral offset [21,55]. Furthermore, as plotted in Fig. 1(d), the AlN film is transparent for H3 but for H5, the absorption length is below 10 nm. Consequently, H3 can pass through but H5 and higher order harmonics like H6 and H7 are absorbed in the film. In Fig. 1(b), the absorbed H5 beam is presented by a

Optics EXPRESS

dashed violet line without an arrow (only H5 is depicted for better visibility). The harmonics, however can also be generated at the AlN-sapphire interface. In contrast to the reflected H5 (also H4, H6, H7), which is absorbed in the AlN film, the transmitted H5 can pass through the sapphire substrate. The absorption length of the used VUV grade sapphire is larger than 1 mm at wavelengths longer than 140 nm [54]; it is out of the plotted range of Fig. 1(d), and even conventional sapphire is transparent at H5 with the used 0.1 mm thickness [56]. It is in line with our observation, where we measured the transmitted H5 in an independent experiment.

Because H5 and higher harmonic orders are situated in the VUV spectral range, the HH source containing the focusing lens, the AlN sample and the focusing mirror were placed inside a vacuum chamber, as shown in Fig. 1(a). A lens with long (500 mm) focal length served as vacuum window to avoid parasitic reflections. The chamber was filled with He gas at pressure ~0.8 bar, which is completely transparent in the VUV spectral range. This was necessary to avoid an undesirable heating processes in the film. The reflected HH beam from the sample was directed to the VUV spectrograph (McPherson 234/302) by two VUV mirrors. Because of the tight focusing of the laser beam needed to reach the ~TW/cm^2 intensity on the AlN sample, the HH beams are highly divergent and refocusing with a VUV grade MgF_2 lens (f = 100 mm) onto the input slit of the VUV spectrograph was needed. The spectrograph was equipped with a 1200 g/mm grating for higher resolution measurements or with a 300 g/mm grating, when higher signal was preferred over resolution. We detected our spectrally resolved HH signal with a photomultiplier tube (Hamamatsu R6836), sensitive in the relevant 115-320 nm spectral range. Its low operation pressure below μbar was ensured with another vacuum pump and with a separating VUV grade MgF_2 window. To enhance the rate of higher order harmonics and to suppress the fundamental and the H3 beams in the measured spectra, it was possible to insert a VUV bandpass filter (130-BB-1D, Pelham Research Optical L.L.C.) before the entrance of the spectrograph (see Fig. 1(a)).

3. Characterization of the intra-oscillator HH source

3.1. Optimization of the system

First we optimized the oscillator without the second focus (see Fig. 1(a), green bold letters, L, AlN, FM). The lens and curved mirror were replaced with a plain high-reflector and BK7 glass was inserted to imitate the dispersion of the lens. The oscillator cavity was optimized for reaching Kerr-lens mode locking (KML), then the lens with the curved mirror was built in to create the second focus. Then, the oscillator was optimized as follow: Appropriately choosing the distance between the lens and the curved end-mirror by means of positioning the lens, optimal continuous wave (CW) operation was achieved. At the optimized CW power, the laser operated at a wavelength between 780 and 790 nm. To restart mode locking, the lens should have been moved closer to the end mirror, which tuned the CW to shorter wavelength of 740-750 nm, as a consequence of the chromatic dispersion of the lens (shorter focal length at shorter wavelength). While the focal length of the lens was shortened due to the Kerr lensing caused by the high peak intensities of the short laser pulses in the cavity, the KML could be started at a somewhat longer wavelength and the spectrum was broad when the cavity dispersion was suitably balanced. After placing the AlN sample as the solid HH source into the secondary focus, the lens position needed slight readjustment and the pump power was increased to compensate the small loss (estimated below 1%) caused by the HH source.

To reach the required short laser pulses in the second focus, the pulses should not be chirped when interacting with the AlN film. The GDD between the arms of the oscillator had to be distributed accordingly. To determine the optimal distribution, first the H3 beam, later the H5 beam was monitored. The strongest signal was reached, when 2 reflections on the chirped mirrors in the short arm and 12 reflections in the long arm were applied as indicated in Fig. 1(a).

Optics EXPRESS

3.2. Characterization of the oscillator

By appropriately turning the pellicle in the cavity, the operational spectrum of the oscillator could be tuned as plotted in the inset of Fig. 2 for three cases, denoted by 750 nm, 775 nm and 800 nm. We characterized the oscillator output using autocorrelation, beyond the output coupler (see Fig. 1(a)). The substrate dispersion of the output coupler was compensated by multiple reflections on chirped mirrors. The measured autocorrelation curves are plotted in Fig. 2, where the optimal compensation of approx. 320 fs^2 was used for the measurements. The measured pulse durations were between 17 fs and 18.5 fs dependent on the selected wavelength. As can be observed from the measured curves, some higher order dispersion remained uncompensated. This is expected, because the intracavity chirped mirrors compensate only the GDD and the higher order contributions of the Ti:sapphire crystal and the lens remain uncompensated. An effect on the complex spectral shape can also be observed. The two spectral maxima separated by approx. 40-50 nm (approx. 20-25 THz), and the corresponding approx. 40-50 fs time interval can be observed in the autocorrelation curves as an additional feature at their pedestals.

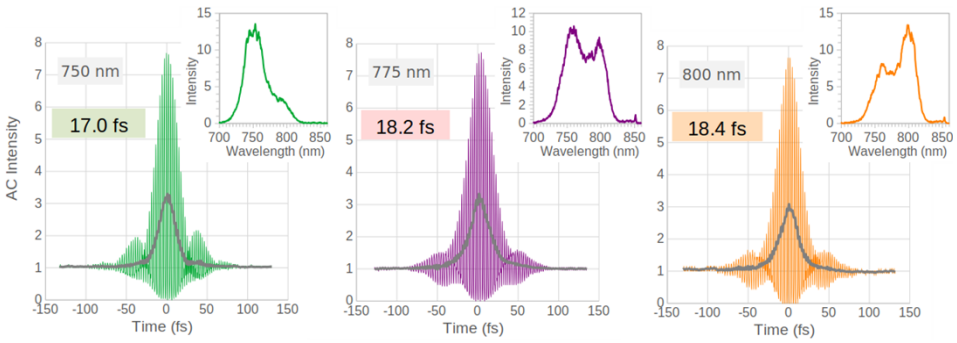

Fig. 2. The measured autocorrelation curves and spectra of the oscillator output at three spectral shapes tuned by the pellicle. Gray lines show the integrated signal over the interference period. The measured beam was extracted from the cavity through the 1% OC mirror and the dispersion caused by its substrate was compensated by multiple reflections on a chirped mirror pair.

3.3. Characterization of the tunable VUV source

As demonstrated in the previous section, the oscillator is tunable between 750 nm and 800 nm by shifting the shape and the spectral center of mass of the generated broad spectra (see insets of Fig. 2 and in Fig. 3(a)). The spectral shape of the harmonics should not strictly follow the shape of the laser spectrum, but its central wavelength should change when the laser spectrum changes because the spectral fields of the high order harmonics can be described as a high order convolution integral of the laser spectral field. We performed the measurements using a 7 nm thick AlN thin film on a 0.1 mm sapphire substrate as source. The measured harmonic spectra are presented in Fig. 3(b) and 3(c) for the third and the fifth harmonic, respectively. The corresponding spectra of the laser and its harmonics are denoted by the same colors. H5 was measured without using the VUV filter while H3 was measured using the filter to suppress the signal below saturation. We observe that both H3 and H5 are tunable; the intensity of H5 is strongly dependent on the generating spectral shape, while the dependence of H3 is much weaker. In both cases, the strongest signals were obtained from the “red” spectrum. In the cases of the “red” and “orange” spectra, the intracavity power was 7.5 W; in the case of “blue” spectrum it reached even 8 W, while for the “green” spectrum, it was only 6 W.

Optics EXPRESS

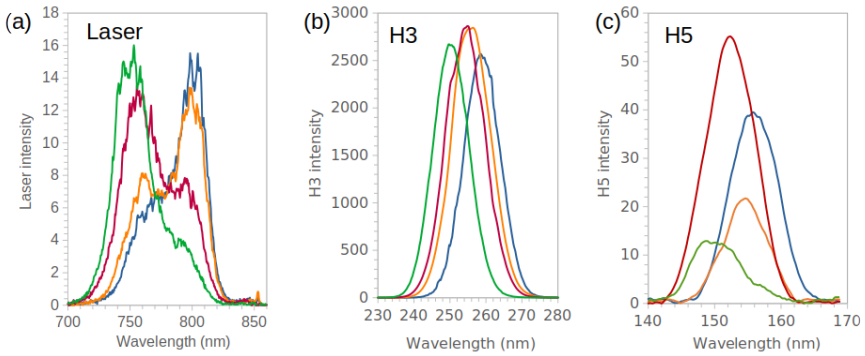

Fig. 3. (a) The tuning the oscillator's operational spectrum (Laser) tuned the harmonic spectra both (b) in the deep ultraviolet via the to 3rd harmonic (H3) and (c) in the VUV via the 5th harmonic (H5). Different colors indicate the corresponding spectra.

Except the "green" spectrum, in the range of 3.8-4 W pump, both the intracavity laser power and also the harmonic powers were independent of the pump power. In the case of "green" spectrum, it was necessary to decrease the pump power to 3.6 W to avoid the appearance of a CW contribution, which resulted in a lower intracavity power. The weaker harmonic power for the "green" spectrum is a direct consequence of the lower intracavity power. Taking the spectroscopically usable power as 10% of the maximum, the VUV source has a usable spectral range between 145 nm and 163 nm.

4. HH source performance using different AlN film thicknesses

It is imperative to understand the effects of the nonlinear AlN film source on the operation of the oscillator and in consequence on the HH process itself. AlN has a large nonlinear refractive index ($n_2 = 1.7 \cdot 10^{-16}$ m^2/W) compared to the sapphire substrate ($n_2 = 3 \cdot 10^{-20}$ m^2/W) [57]. In the secondary focus, where it is placed, the laser intensity is large, and produces additional parasitic Kerr-lensing in the cavity, which can take part in the KML operation. To study this, several AlN film thicknesses were tested and even a sapphire substrate was used too without any AlN film, as a reference. The generated spectra are plotted in Fig. 4.

In the case of the pure sapphire substrate, Fig. 4(a), only H3 is generated and no other harmonics. With 7 nm AlN film, Fig. 4(b), beyond H3, strong H5 is generated and even a weaker H4 and H6 can be seen. Because AlN is weakly birefringent in the c-axes direction [58], the appearance of the even harmonics can be expected at non-normal incidence angles for "as-deposited" films [59]. The measured spectrum also shows the second diffraction order of H5 at the position of H5/2. The intensity of H3 is comparable to that generated on the substrate alone. Using thicker AlN film of 100 nm, Fig. 4(c), essential differences can be observed. The H5 is somewhat weaker, compared to 7 nm AlN film, but H4 is much stronger. Even H3 is much stronger and beyond a somewhat stronger H6, the H7 is well visible. The second diffraction order of H5 (H5/2) and the second and third diffraction order of H7 (H7/2, H7/3) can be also recognized. Additionally, a continuum background appears, denoted by the orange dashed curve. This continuum background will be discussed in the next chapter.

Using even thicker, 300 nm AlN film, higher order harmonics as H4, H5, H6 are much weaker and H3 remains strong. Moreover, we find that the film thickness itself affects the operation of the oscillator. While with a 7 nm film, 7.0-7.5 W intracavity power is obtained, this decreases to 6.5-7.0 W using a 100 nm film and even to 6 W in the case of a 300 nm film. The significantly decreased intracavity power in the case of the 300 nm film can explain the much weaker higher order harmonics and the decreased continuum background.

Optics EXPRESS

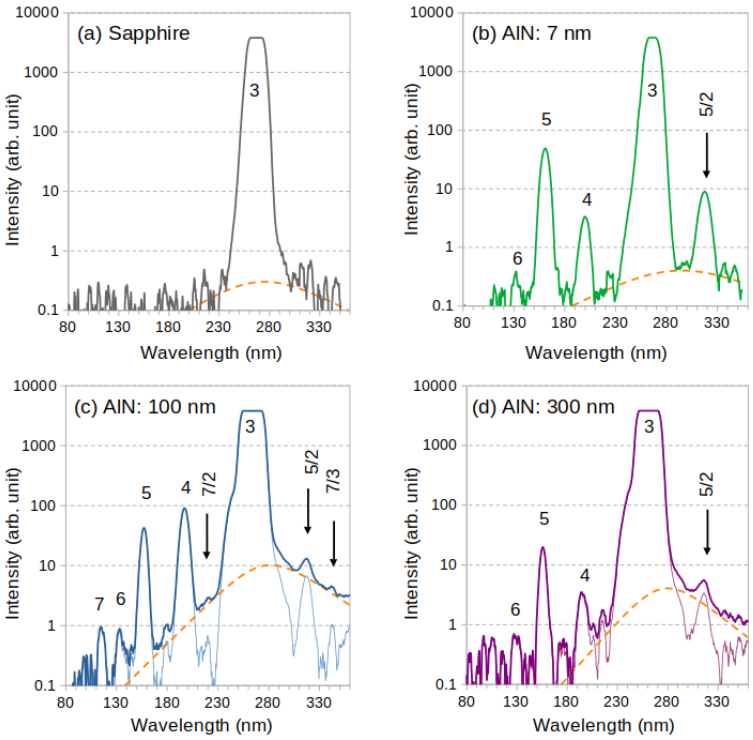

Fig. 4. Measured reflected HH spectra, generated using different AlN film thicknesses on sapphire substrate (b,c,d). The spectrum from the substrate without AlN film is also measured for reference (a). The intensity scales are comparable among the figure panels. The super-continuum backgrounds are denoted in dashed orange lines. For 100 nm and 300 nm AlN thickness, the spectra after subtracting the continuum background are plotted with thinner lines. In all panels, H3 saturated the detector.

5. Coherent continuum background

We observe continuum backgrounds beyond the harmonic lines in the generated spectra, as seen in Fig. 4. The origin of these backgrounds is not straightforward. It was the strongest for the 100 nm AlN film, but it can also be seen for a 7 nm film and it is still strong in the case of 300 nm film. Important observations can be made, which suggest that this background is coherent. It can be concluded, if the intensity of one of the harmonic lines is comparable to the continuum background, and spectral interference becomes visible. In Fig. 5, we illustrate observations of such spectral interference fringes. In Fig. 5(a), the intracavity dispersion was still not optimized and H5 was relative weak, but larger than the background. Higher order harmonics were not generated. Interference fringes with approx. 70 THz period can be seen. A fitted curve expecting Gaussian harmonic line shape $A(\nu)$ is plotted using the form $I(\nu) = I_0[A^2(\nu) + Q^2 + 2QA(\nu)cos(2\pi\nu/\Delta\nu + \phi)]$ counting with the spectral period $\Delta\nu$ and the rate of the electric fields $Q = E_{SPM}/E_{HH}$. At optimized intracavity dispersion, in Fig. 5(b) and 5(c), interference fringes in the spectra of H6 and H7 can be observed with approx. 60 THz periods.

For the origin of the coherent background continuum, we suggest the following explanation. Harmonics are generated by nonlinear interaction. The third order nonlinear polarization contains

Optics EXPRESS

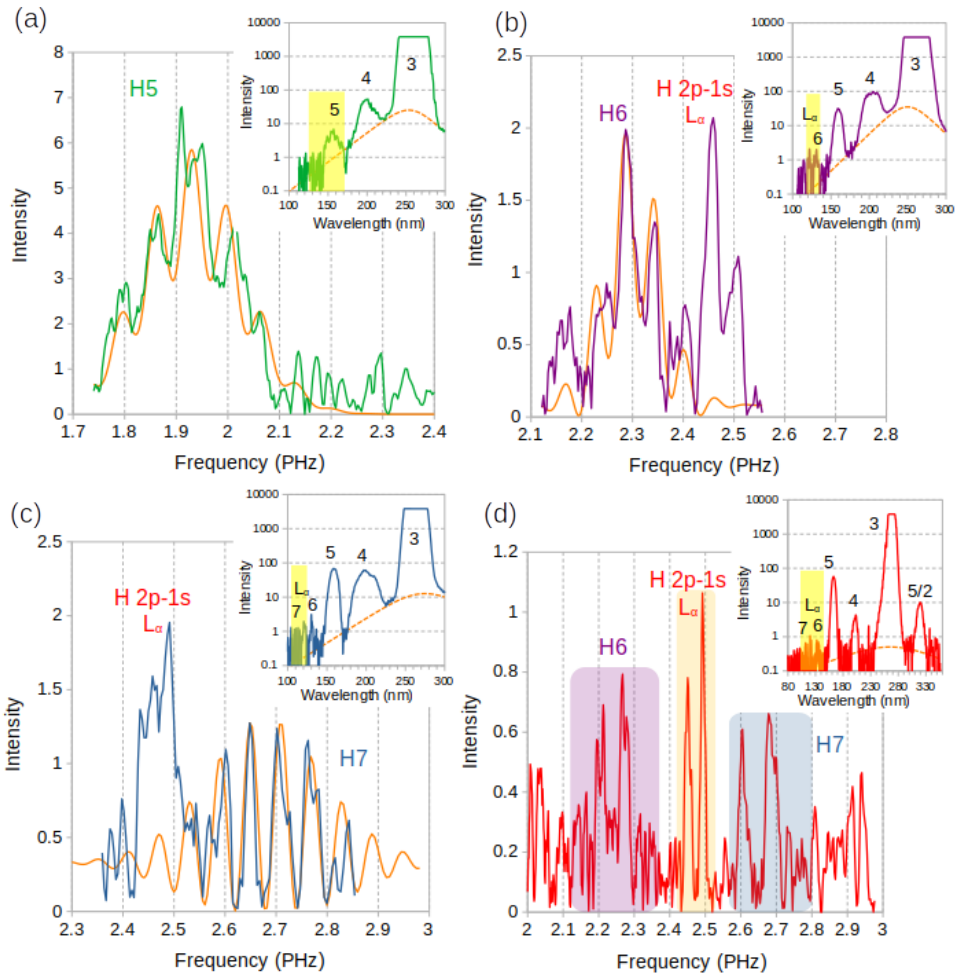

Fig. 5. Spectral interference was observed between the generated harmonic lines and the coherent background continuum for (a) H5, (b) H6 and (c) H7. The fitted interference patterns are plotted with orange solid lines using fitting parameters like spectral periods: 70, 60, 60 THz; rate of the electric fields: Q = 0.18, 0.25, 1.0; phases: -2, -0.5, -1 rad. Beyond the harmonic lines, the spectral line of the hydrogen 2p-1s transition at 121.5 nm is also visible. (d) The H6-H7 spectral range was measured with higher spectral resolution. In the insets, the full measured spectra are plotted; the coherent background is denoted by orange dashed lines, and yellow highlighted spectral ranges are plotted in detail. In the insets, H3 saturated the detector.

two terms, the self-phase modulation (SPM) and the third harmonic generation (3HG).

$$\text{SPM:} \qquad P_{NL}(\omega) \propto 3\chi^{(3)}E^2(\omega)E(-\omega), \tag{3}$$

$$\text{3HG:} \qquad P_{NL}(3\omega) \propto \chi^{(3)}E^3(\omega). \tag{4}$$

SPM, due to the $\omega = \omega + \omega - \omega$ process, produces a broad coherent pedestal of the fundamental laser spectrum, which can be observed as the coherent super-continuum background. These are plotted in orange dashed lines in Fig. 4. The short wavelength slope is given by the pedestal of the super-continuum, while the long wavelength slope is defined by the spectral sensitivity of the photomultiplier. Harmonics are generated similarly to Eq. (4) for any harmonics, HHG:

Optics EXPRESS

$P_{NL}(q\omega) \propto \chi^{(q)}E^q(\omega)$ perturbative or mainly non-perturbative manner, depending on the laser intensity. If the intensity of the super-continuum background is comparable to the intensity of a harmonic line, spectral interference can be observed. The 60-70 THz period of the spectral interference pattern suggest a time difference of 14-17 fs between the generation of coherent background and the generation of harmonics. It is feasible, because the maximum of the SPM is generated at the maximum of the laser pulse or moves somewhat due to the dispersion of the third-order susceptibility, while for non-perturbative HH generation, the electrons should be moved to the conduction band by tunnel or multi-photon excitation; the excitation timescale is integrated over the laser pulse and consequently delayed, and the observed difference is similar to the pulse duration.

In both figures of 5(b) and 5(c), beyond the harmonic lines, an additional narrower line between 2.4 and 2.5 PHz appeared. For identifying this line, a spectrum with higher resolution (1200 g/mm grating instead of 300 g/mm and 1 nm/s scanning speed instead of the usual 2 nm/s) was recorded in Fig. 5(d). In that case, the signal is weaker, near the single photon detection mode, but both H6 and H7 can be seen together with the extra line. This line is identified as the Lyman α line of the hydrogen 2p – 2s transition, which should be at 2.47 PHz (121.5 nm). We suspect the hydrogen to originate from residual water vapor in the vacuum chamber and the water molecules were broken and excited by the strong H3 beam in multi-photon absorption.

6. Conclusion and prospects

We developed a very compact VUV laser source by integrating the HH source into the cavity of a mode-locked, femtosecond, Ti:sapphire oscillator. The source is running at 80 MHz, a much higher repetition rate than previous realizations of intra-cavity HH generation. An AlN film coated on a thin sapphire substrate is used as a solid HH source and the harmonics are generated due to nonlinear reflection on the thin film, which eliminates the need for a separate output coupler for the VUV beam. Furthermore, as a consequence of the nonlinear reflection, we observed a weak, broad and coherent super-continuum and its interference with harmonic lines when their intensities become comparable.

The concept has been successfully demonstrated and a highly compact, high repetition rate, coherent vacuum ultraviolet light source has been realized with a spectrum reaching up to the 7th harmonics. The harmonic lines are tunable and the 5th harmonic covers the range between 145 and 163 nm, which makes this source suitable for laser spectroscopy of the ^{229m}Th isomer nuclear transition.

We produce a power in the range of few-nW to sub-nW in the 5th harmonic. Higher power was achieved only with dramatically more complex, enhancement cavity extended, large fiber laser systems and with lower repetition rate thin disk oscillators. At this moment, the main limitation for our source to reach higher VUV power is the heating of the solid sample due to multi-photon absorption in the AlN film, which limits the intracavity power to approx. 8 W compared to the kW level of other systems. The increased temperature can strongly influence the properties of the AlN films [60] and even can damage it. The estimated fluence in the focus is approx. 0.1 J/cm^2, which is more than one order of magnitude smaller than the damage threshold of the AlN and the sapphire [61]. By increasing the intracavity power only by a factor of 4, the power of the 5th harmonic can reach the μW regime, which is approaching the power requirement of ^{229}Th isomer spectroscopy [5,8] or becomes suitable to reference narrow linewidth lasers used for its spectroscopy. Therefore, we are convinced that the output VUV power can be increased by orders of magnitudes by implementing an efficient cooling of the AlN film and consequentially raising the intracavity power.

Funding. Federación Española de Enfermedades Raras (FICTS2019-02-40); Österreichische Nationalstiftung für Forschung, Technologie und Entwicklung (AQUnet); European Metrology Programme for Innovation and Research (20FUN01 TSCAC); HORIZON EUROPE European Research Council (856415).

Optics EXPRESS

Acknowledgment. We are grateful for sample preparation and characterization to E. Céspedes and M. Zabala.

Disclosures. The authors declare no conflicts of interest.

Data availability. Data underlying the results presented in this paper are not publicly available at this time but may be obtained from the authors upon reasonable request.

References

1. C.-T. Chiang, A. Blättermann, M. Huth, *et al.*, "High-order harmonic generation at 4 MHz as a light source for time-of-flight photoemission spectroscopy," Appl. Phys. Lett. **101**(7), 071116 (2012).
2. C. Corder, P. Zhao, J. Bakalis, *et al.*, "Ultrafast extreme ultraviolet photoemission without space charge," Struct. Dyn. **5**(5), 054301 (2018).
3. K. Wakui, K. Hayasaka, and T. Ido, "Generation of vacuum ultraviolet radiation by intracavity high-harmonic generation toward state detection of single trapped ions," Appl. Phys. B **117**(3), 957–967 (2014).
4. B. Seiferle, L. von der Wense, P. V. Bilous, *et al.*, "Energy of the ^{229}Th nuclear clock transition," Nature **573**(7773), 243–246 (2019).
5. L. von der Wense and C. Zhang, "Concepts for direct frequency-comb spectroscopy of ^{229m}Th and an internal-conversion-based solid-state nuclear clock," Eur. Phys. J. D **74**(7), 146 (2020).
6. T. Sikorsky, J. Geist, D. Hengstler, *et al.*, "Measurement of the ^{229}Th isomer energy with a magnetic microcalorimeter," Phys. Rev. Lett. **125**(14), 142503 (2020).
7. E. Peik, T. Schumm, M. S. Safronova, *et al.*, "Nuclear clocks for testing fundamental physics," Quantum Sci. Technol. **6**(3), 034002 (2021).
8. C. Zhang, P. Li, J. Jiang, *et al.*, "Tunable VUV frequency comb for ^{229m}Th nuclear spectroscopy," Opt. Lett. **47**(21), 5591–5594 (2022).
9. A. Schönberg, H. S. Salman, A. Tajalli, *et al.*, "Below-threshold harmonic generation in gas-jets for Th-229 nuclear spectroscopy," Opt. Express **31**(8), 12880–12893 (2023).
10. S. Kraemer, J. Moens, M. Athanasakis-Kaklamanakis, *et al.*, "Observation of the radiative decay of the ^{229}Th nuclear clock isomer," Nature **617**(7962), 706–710 (2023).
11. K. Scharl, S. Ding, G. Holthoff, *et al.*, "Setup for the ionic lifetime measurement of the $^{229m}Th^{3+}$ nuclear clock isomer," Atoms **11**(7), 108 (2023).
12. A. K. Mills, T. J. Hammond, M. H. C. Lam, *et al.*, "XUV frequency combs via femtosecond enhancement cavities," J. Phys. B **45**(14), 142001 (2012).
13. I. Pupeza, C. Zhang, M. Högner, *et al.*, "Extreme-ultraviolet frequency combs for precision metrology and attosecond science," Nat. Photonics **15**(3), 175–186 (2021).
14. A. Ermolov, K. F. Mak, M. H. Frosz, *et al.*, "Supercontinuum generation in the vacuum ultraviolet through dispersive-wave and soliton-plasma interaction in a noble-gas-filled hollow-core photonic crystal fiber," Phys. Rev. A **92**(3), 033821 (2015).
15. T. Kanai, T. Kanda, T. Sekikawa, *et al.*, "Generation of vacuum-ultraviolet light below 160 nm in a KBBF crystal by the fifth harmonic of a single-mode Ti:sapphire laser," J. Opt. Soc. Am. B **21**(2), 370–375 (2004).
16. T. Nakazato, I. Ito, Y. Kobayashi, *et al.*, "Phase-matched frequency conversion below 150 nm in $KBe_2BO_3F_2$," Opt. Express **24**(15), 17149–17158 (2016).
17. W. Ubachs, K. S. E. Eikema, and W. Hogervorst, "Narrow-band extreme-ultraviolet laser radiation tunable in the range 90.5–95 nm," Appl. Phys. B **57**(6), 411–416 (1993).
18. R. R. Freeman, G. C. Bjorklund, N. P. Economou, *et al.*, "Generation of cw VUV coherent radiation by four-wave sum frequency mixing in Sr vapor," Appl. Phys. Lett. **33**(8), 739–742 (1978).
19. G. Hilber, A. Lago, and R. Wallenstein, "Broadly tunable vacuum-ultraviolet/extreme-ultraviolet radiation generated by resonant third-order frequency conversion in krypton," J. Opt. Soc. Am. B **4**(11), 1753–1764 (1987).
20. T. Tsang, "Third- and fifth-harmonic generation at the interfaces of glass and liquids," Phys. Rev. A **54**(6), 5454–5457 (1996).
21. H. Kim, S. Han, Y. W. Kim, *et al.*, "Generation of Coherent Extreme-Ultraviolet Radiation from Bulk Sapphire Crystal," ACS Photonics **4**(7), 1627–1632 (2017).
22. J. Seres, E. Seres, C. Serrat, *et al.*, "Non-perturbative generation of DUV/VUV harmonics from crystal surfaces at 108 MHz repetition rate," Opt. Express **26**(17), 21900–21909 (2018).
23. Y. Kobayashi, N. Hirayama, A. Ozawa, *et al.*, "10-MHz, Yb-fiber chirped-pulse amplifier system with large-scale transmission gratings," Opt. Express **21**(10), 12865–12873 (2013).
24. F. Emaury, A. Diebold, C. J. Saraceno, *et al.*, "Compact extreme ultraviolet source at megahertz pulse repetition rate with a low-noise ultrafast thin-disk laser oscillator," Optica **2**(11), 980–984 (2015).
25. C. Gohle, T. Udem, M. Herrmann, *et al.*, "A frequency comb in the extreme ultraviolet," Nature **436**(7048), 234–237 (2005).
26. R. J. Jones, K. D. Moll, M. J. Thorpe, *et al.*, "Phase-coherent frequency combs in the vacuum ultraviolet via high-harmonic generation inside a femtosecond enhancement cavity," Phys. Rev. Lett. **94**(19), 193201 (2005).
27. J. Lee, D. R. Carlson, and R. J. Jones, "Optimizing intracavity high harmonic generation for XUV fs frequency combs," Opt. Express **19**(23), 23315–23326 (2011).

Optics EXPRESS

28. G. Winkler, J. Fellinger, J. Seres, *et al.*, "Non-planar femtosecond enhancement cavity for VUV frequency comb applications," Opt. Express **24**(5), 5253–5262 (2016).
29. J. Seres, E. Seres, C. Serrat, *et al.*, "All-solid-state VUV frequency comb at 160 nm using high-harmonic generation in nonlinear femtosecond enhancement cavity," Opt. Express **27**(5), 6618–6628 (2019).
30. D. C. Yost, T. R. Schibli, J. Ye, *et al.*, "Vacuum-ultraviolet frequency combs from below-threshold harmonics," Nature Phys. **5**(11), 815–820 (2009).
31. A. Ozawa, Z. Zhao, M. Kuwata-Gonokami, *et al.*, "High average power coherent vuv generation at 10 MHz repetition frequency by intracavity high harmonic generation," Opt. Express **23**(12), 15107–15118 (2015).
32. J. Zhang, L.-Q. Hua, Z. Chen, *et al.*, "Extreme ultraviolet frequency comb with more than 100 μW average power below 100 nm," Chin. Phys. Lett. **37**(12), 124203 (2020).
33. E. Seres, J. Seres, and C. Spielmann, "Extreme ultraviolet light source based on intracavity high harmonic generation in a mode locked Ti:sapphire oscillator with 9.4 MHz repetition rate," Opt. Express **20**(6), 6185–6190 (2012).
34. F. Labaye, M. Gaponenko, V. J. Wittwer, *et al.*, "Extreme ultraviolet light source at a megahertz repetition rate based on high-harmonic generation inside a mode-locked thin-disk laser oscillator," Opt. Lett. **42**(24), 5170–5173 (2017).
35. J. Fischer, J. Drs, F. Labaye, *et al.*, "Intra-oscillator high harmonic generation in a thin-disk laser operating in the 100-fs regime," Opt. Express **29**(4), 5833–5839 (2021).
36. A. A. Eilanlou, T. Okino, Y. Nabekawa, *et al.*, "Observation of harmonic beams inside a Kerr lens mode-locked thin-disk ring laser oscillator beyond a repetition rate of 10 MHz," OSA Continuum **4**(3), 1099–1112 (2021).
37. J. Fischer, J. Drs, F. Labaye, *et al.*, "Efficient XUV-light out-coupling of intra-cavity high harmonics by a coated grazing-incidence plate," Opt. Express **30**(17), 30969–30979 (2022).
38. O. Pronin, V. Pervak, E. Fill, *et al.*, "Ultrabroadband efficient intracavity XUV output coupler," Opt. Express **19**(11), 10232–10240 (2011).
39. K. D. Moll, R. J. Jones, and J. Ye, "Output coupling methods for cavity-based high-harmonic generation," Opt. Express **14**(18), 8189–8197 (2006).
40. I. Pupeza, S. Holzberger, T. Eidam, *et al.*, "Compact high-repetition-rate source of coherent 100 eV radiation," Nat. Photonics **7**(8), 608–612 (2013).
41. D. C. Yost, T. R. Schibli, and J. Ye, "Efficient output coupling of intracavity high-harmonic generation," Opt. Lett. **33**(10), 1099–1101 (2008).
42. I. Pupeza, M. Högner, J. Weitenberg, *et al.*, "Cavity-Enhanced High-Harmonic Generation with Spatially Tailored Driving Fields," Phys. Rev. Lett. **112**(10), 103902 (2014).
43. C. Zhang, S. B. Schoun, C. M. Heyl, *et al.*, "Noncollinear enhancement cavity for record-high out-coupling efficiency of an extreme-UV frequency comb," Phys. Rev. Lett. **125**(9), 093902 (2020).
44. N. Bloembergen and P. S. Pershan, "Light waves at the boundary of nonlinear media," Phys. Rev. **128**(2), 606–622 (1962).
45. D. J. Moss, H. M. van Driel, and J. E. Sipe, "Third harmonic generation as a structural diagnostic of ion-implanted amorphous and crystalline silicon," Appl. Phys. Lett. **48**(17), 1150–1152 (1986).
46. T. Y. F. Tsang, "Optical third-harmonic generation at interfaces," Phys. Rev. A **52**(5), 4116–4125 (1995).
47. G. Vampa, Y. S. You, H. Liu, *et al.*, "Observation of backward high-harmonic emission from solids," Opt. Express **26**(9), 12210–12218 (2018).
48. P. Suthar, F. Trojánek, P. Malý, *et al.*, "Role of Van Hove singularities and effective mass anisotropy in polarization-resolved high harmonic spectroscopy of silicon," Commun. Phys. **5**(1), 288 (2022).
49. J. Seres, E. Seres, E. Céspedes, *et al.*, "Probing nonperturbative third and fifth harmonic generation on silicon without and with thermal oxide layer," J. Opt. **25**(10), 105501 (2023).
50. J. Seres, E. Seres, E. Céspedes, *et al.*, "Nonperturbative generation of harmonics by nanometer-scale localized electronic states on the surface of bulk materials and nano-films," Optics **4**(1), 246–257 (2023).
51. D. Kecik, C. Bacaksiz, R. T. Senger, *et al.*, "Layer- and strain-dependent optoelectronic properties of hexagonal AlN," Phys. Rev. B **92**(16), 165408 (2015).
52. E. Seres, J. Seres, and T. Schumm, "Group delay dispersion tuned femtosecond Kerr-lens mode-locked Ti:sapphire laser," Opt. Continuum **1**(4), 860–865 (2022).
53. T. Brabec, P. F. Curley, C. Spielmann, *et al.*, "Hard-aperture Kerr-lens mode locking," J. Opt. Soc. Am. B **10**(6), 1029–1034 (1993).
54. M. E. Innocenzi, R. T. Swimm, M. Bass, *et al.*, "Room-temperature optical absorption in undoped α-Al_2O_3," J. Appl. Phys. **67**(12), 7542–7546 (1990).
55. J. Seres, E. Seres, C. Serrat, *et al.*, "High harmonic generation in AlN due to out-of-surface electron orbitals," OSA Continuum **4**(1), 47–54 (2021).
56. S. Kawaminami, K. Mochizuki, N. Adachi, *et al.*, "Crystal growth of large sapphire and its optical properties," J. Ceram. Soc. Jpn. **122**(1428), 695–700 (2014).
57. M. Zhao, C.-H. Xu, W.-J. Hu, *et al.*, "Observation of two-photon absorption and nonlinear refraction in AlN," Chinese Phys. Lett. **33**(10), 104201 (2016).
58. S. R. Bowman, C. G. Brown, and B. Taczak, "Optical dispersion and phase matching in gallium nitride and aluminum nitride," Opt. Mater. Express **8**(4), 1091–1099 (2018).
59. T. Journigan, Y. Liu, C. Cabello, *et al.*, "High harmonic generation in epitaxially grown zinc oxide films," J. Opt. Soc. Am. B **41**(6), B1–B6 (2024).

Optics EXPRESS

60. M. Feneberg, M. F. Romero, B. Neuschl, *et al.*, "Temperature dependent dielectric function and reflectivity spectra of nonpolar wurtzite AlN," Thin Solid Films **571**, 502–505 (2014).
61. F. Preusch, B. Adelmann, and R. Hellmann, "Micromachining of AlN and Al_2O_3 Using Fiber Laser," Micromachines **5**(4), 1051–1060 (2014).